

Meshfree Digital Total Variation Based Algorithm for Multiplicative Noise Removal*

MUSHTAQ AHMAD KHAN, WEN CHEN[†], ZHOUJIA FU[†]
AND ASMAT ULLAH

*State Key Laboratory of Hydrology-Water Resources and Hydraulic Engineering
College of Mechanics and Materials*

Hohai University

Jiangsu, 210098 P.R. China

E-mail: {[†]d2014017; [†]chenwen; paul212063}@hhu.edu.cn; asmatullah75@gmail.com

The Digital Total Variation (DTV) filtering is a digitized energy method used to denoise the measured image data. Different from the traditional variation method, this technique applies to arbitrarily located data points and also has the built-in edge detective property. This paper introduces a novel meshfree algorithm (Kansa technique) using DTV method and Radial Basis Functions (RBFs) approximation for the numerical solution of the DTV-based model to remove the multiplicative noise from the measurements. This approach is structured on local collocations and multiquadric radial basis function. These features enable this method to eliminate noise from images while sharply resolving discontinuities. It is observed that the present methodology is fast, robust, and computationally efficient, requires simple post-processing, and can be easily implemented. The numerical experiments show that the proposed method performs well in visual improvement as well as peak signal-to-noise ratio compared with the recent total variation partial differential equation (PDE)-based methods for multiplicative noise removal.

Keywords: image denoising, digital total variation (DTV) filter, multiquadric radial basis function (MQ RBF), restoration equation, mesh method, meshfree method

1. INTRODUCTION

In recent decades, the researchers have done a lot of work in the area of image denoising, in particular, on additive noise removal problems. However, there is another more complex noise called multiplicative noise. In this study, we focus on such multiplicative noise removal problems, which can be stated as

$$f = u \eta_1, \quad (1)$$

where u is the original image and $f: \Omega \subset R^2 \rightarrow R$, is the given noisy image having multiplicative noise η_1 . Here, Ω represents the image the domain which is usually a rectangular area. In this study, we consider a 2-dimensional image having size $M \times N$. We also suppose that each value of u and f have positive values in the noise model. The multiplicative noise vanishes about all the data of the original picture when the noise corrupts the

Received October 15, 2017; revised January 3, 2018; accepted February 6, 2018.

Communicated by Wen-Liang Hwang.

[†] Corresponding authors: d2014017@hhu.edu.cn; chenwen@hhu.edu.cn

* The work described in this paper was supported by the National Natural Science Foundation of China (No. 11702083), the Natural Science Foundation of Jiangsu Province (No. BK20150795), the Fundamental Research Funds for the Central Universities (No. 2018B16714), and the State Key Laboratory of Mechanics and Control of Mechanical Structures (Nanjing University of Aeronautics and Astronautics) (No. MCMS-0218 G01).

original image. Therefore, it is vital to expel the multiplicative noise and to recoup the real picture u from the information data f . The issue of expelling the multiplicative noise happens in numerous applications, for example, synthetic aperture radar (SAR) images, ultrasound images, and laser imagining, see [48]. Multiplicative noise removal methods have been discussed in many reports, for instance, in [20, 29, 55, 57, 58, 61, 62].

In literature, many other approaches have been used to solve the problems having multiplicative noise by taking the logarithmic amplification which transforms multiplicative noise into additive Gaussian-type noise. Popular methods include shrinkage and Bayesian MAP estimator methods [1, 19, 68] and various variational methods [3, 30, 50, 58, 59] and hence many good restoration results have been produced.

Over the last several years, many optimization methods which include fixed-point methods [14, 27], iterative shrinkage-thresholding algorithms [4, 66], the Newton-like methods [45], subspace optimization method [44], and operator splitting methods [6, 13, 23] have proposed for the minimization model in image restoration. Among these methods, the (linearized) Augmented Lagrangian algorithm (ALM), and primal-dual hybrid gradient (PDHG) algorithm are two of the most successful and most widely used techniques. In recent years, the augmented Lagrangian methods [6, 59] were applied to compute the solution of TV-based model efficiently. However, the original ALM requires inner iterations or inverses involving the Laplacian operator who is still time-consuming in each iteration. To improve the efficiency of ALM, the authors used the linearized techniques [11, 12, 67] for better restoration results for multiplicative noise removal. Also, the primal-dual hybrid gradient algorithm [17, 24, 46, 65] based on primal-dual variables [71], gradient descent, and ascent schemes for the solution of TV-based minimization problem for image restoration. But in these approaches, the selection of proper variables and choosing the appropriate values for the parameters used in them are time-consuming and hence create complexity.

The total variation (TV) filtering has proved to be one of the most successful tools in image processing for the solution of variational based partial differential equation (PDE) restoration problems. For more details about the TV filtering, see [47, 48]. Another method is to digitize the whole system. This idea begins with a discrete variational problem and works with data in the general discrete domain, a graph. The digitized approach is more adaptable as irregularly shaped domains, and scattered data points can be taken care of effectively. One understood digitization strategy is digital total variation (DTV) filtering [2, 10]. The DTV procedure can pointedly resolve discontinuities without earlier information of edge locations since it has built-in edge detection [2, 60, 70]. The point qualities might be situated at scattered, non-structured locales in a complex geometry. Not at all like the other pseudo spectral post processing techniques, the DTV strategy does not require data location on the structured grid; therefore, it is a more broad technique. With regards to numerical PDEs, the DTV strategy has already been utilized for the steady-state, mesh-based solutions of conservation of law computed by the second order, Lax-Wendroff methods [2, 8, 9]. The DTV strategy has been proposed and developed in [10, 70] to remove noise and restore accuracy. In recent years, some work has been done on picture denoising having additive noise [10, 70] and arbitrary data points having Gibbs oscillation [52] utilizing DTV filter, and thus, some desirable results have been obtained.

Recent decades have witnessed a lot of work to use the RBFs as the effective basis

function for the interpolation and approximation of multi-variable smooth functions on scattered data sets [25]. More recently, expanding consideration has been given to the development of meshless strategies utilizing RBFs for the numerical solution of PDEs. Most PDE results have concerned steady state issues with smooth solutions. More recently much attention has been given to applying RBF collocation methods to solve the time-dependent PDE problems for the smooth solution. The RBF methods have more points of interest and have exhibited superior accuracy as compared with traditional numerical strategies, for instance, finite difference strategy (FDM) [69], finite element method (FEM) [38], finite volume strategy (FVM) [35, 39], and pseudo-spectral strategy [37]. For information about RBF strategies, see [5, 16, 18, 26, 31, 32, 40].

Global RBF collocation strategy is also simple to execute, gives excellent accuracy and converges exponentially to solve the PDEs. Notwithstanding, in this technique, the interpolation matrix is wholly populated and ill-conditioned, and thus sensitive to the shape parameter. Therefore, it is computationally extremely costly to apply global collocation method to large-scale problems. So in literature, Kansa technique [15, 33] is a domain type collocation strategy to overcome these issues.

The focal motivations behind the energy of the RBFs for interpolating scattered multidimensional data are investigated in [7, 34]. In late decades, meshless techniques have been exhibited to handle scientific and engineering issues. The mesh-less technique based on the collocation strategy has been superior and extremely helpful. Over the last several decades RBFs have been observed to be widely successful for the interpolation of scattered data. RBF techniques are not fixed to a grid and like this, have a place with a class of methods called mesh-less methods. They apply just a cloud of points without any information about nodal connections. It is (conditionally) positive definite [43, 51], rotationally and translationally invariant. The RBF approximation is an exceedingly powerful tool for representing smooth functions in non-trivial geometries since the strategy is mesh-free and can be spectrally accurate [21]. RBFs interpolations have been utilized to expel the Gibbs oscillations, and additive Gaussian noise from the given arbitrary data points and noisy images, and hence beneficial results have been obtained [36, 53]. In this work, we use the Multiquadratic MQ-RBF collocation technique (Kansa strategy) for the solution of the nonlinear PDE arising from the multiplicative noise model functional for smooth restoration results. The Kansa technique is a domain type strategy, which has numerous features like the finite element approach. The DTV filter for multiplicative noise removal problem has not been described.

The rest of the paper is organized as follows. In section 2, some related work including details and applications of DTV in image restoration is presented. This section also includes the details of RBFs and its applications in solving PDEs. Section 3 discusses the HMW [30] model used for the multiplicative noise removal. The proposed method which is DTV method using RBF collocation method (Kansa method) has been explained in section 4. Section 5 describes experimental results and discussion to compare the two models regarding CPU times, the number of iterations, and visual quality of restoration (Peak Signal to Noise Ratio (PSNR)) of the restored images. This section also includes the shape parameter analysis on image restoration. Section 6 contains the comparison of our proposed method with other variational based methods for image restoration. Section 7 shows the tabulated discussions about the sensitivity of the parameters of the proposed method. The conclusion is provided in section 8.

2. RELATED WORK

2.1 Digital Total Variation Filtering

Let us describe the DTV method [2]. The DTV filtering applies on a general graph with $[\Omega, D]$, *i.e.*, finite set Ω vertices (or nodes/pixels) and a directory, D , of edges. Also, it is supposed that the graph is associated and has no self-loops (no immediate edge from a vertex to itself). General vertices are indicated by α, β, \dots . The notation $\alpha \sim \beta$ demonstrates that α and β are neighbors. All the neighbors of α are denoted by

$$N_\alpha = \{\beta \in \Omega / \beta \sim \alpha\} \text{ for } \alpha \sim \beta \equiv \beta \sim \alpha.$$

A digital image, u is a function $u: \Omega \rightarrow R$, where u_α signify the value of u at vertex α . At any vertex α , the regularized local variation or strength function $\|\nabla_p u_\alpha\|$ is characterized as

$$\|\nabla_p u_\alpha\| := \left(\sum_{\beta \in N_\alpha} (u_\beta - u_\alpha) \right)^{\frac{1}{2}}.$$

For any positive number a , the regularized location variation or strength function can be re-defined as

$$\|\nabla_p u_\alpha\| := \left(a^2 + \sum_{\beta \in N_\alpha} (u_\beta - u_\alpha) \right)^{\frac{1}{2}},$$

where a is a small regularized parameter to avoid the regularized local variation from zero denominator.

As discussed in [2], the edge derivative of u along e can be defined as

$$\left. \frac{\partial u}{\partial e} \right|_\alpha := u_\beta - u_\alpha,$$

where e is called the edge and represents the edge $\alpha \sim \beta$.

$$\text{Apparently, } \left. \frac{\partial u}{\partial e} \right|_\alpha = - \left. \frac{\partial u}{\partial e} \right|_\beta \text{ and } \|\nabla_p u_\alpha\| = \sqrt{\sum_{e^+ \alpha} \left[\left. \frac{\partial u}{\partial e} \right|_\alpha \right]^2}$$

where $e^+ \alpha$ represents that α is one node of e .

The first DTV-based model for image restoration having additive noise was proposed and presented by T. F. Chan, *et al.*, [10] in 2001. Noisy image for this model is modeled (for additive noise) as

$$u_0 = u + \eta \text{ or } u_\alpha^0 = u_\alpha + \eta_\alpha \text{ for all } \alpha \in \Omega, \quad (2)$$

where u_0 is noisy data, u is the required clean data and η is the noisy data. The minimization approach for Eq. (2) is given as under

$$\min_u E(u) = \sum_{\alpha \in \Omega} \|\nabla_p u_\alpha\|_a + \frac{\lambda}{2} \|u_\alpha - u_\alpha^0\|_\Omega^2 \text{ for all } \alpha \in \Omega, \tag{3}$$

where the first term is called the regularization term, the second term is called the data fidelity term, λ is the fitting parameter, and a is the regularized parameter.

2.2 Radial Basis Functions Approximation

RBFs are multivariate functions, and the values rely on upon the detachment from the point of departure called center, so that $\phi(x) = \phi(r) \in R, x \in R^n, r \in R$; or identically on the separation from a state of a given set $\{x_j\}$ to such a degree, to the point that $\phi(x - x_j) = \phi(r_j) \in R$. Any function ϕ fulfilling the property $\phi(x) = \phi(\|x\|_2)$ is known as the radial function. Some examples of commonly used RBFs are given in Table 1.

For a continuous multivariate function $f(x), x \in \Omega \subseteq R^n$ is the bounded domain, RBF interpolation for N interpolation function values $\{y_i\}_{i=1}^N$ at the data location (which are called centers in the RBF concept) $\{x_i\}_{i=1}^N \in \Omega \subseteq R^n$, can be written as linear combination of RBFs, specifically,

$$f(x) = \sum_{j=1}^N \gamma_j \phi(\|x - x_j\|_2), x \in \Omega \tag{4}$$

where γ_j are unknown RBF coefficients which must be determined [15]. Using the collocation method, one may write:

$$y_i = f(x_i) = \sum_{j=0}^N \gamma_j \phi(\|x_i - x_j\|_2), i, j = 1, 2, 3, \dots, N.$$

The above linear system of equations for RBF coefficients can be re-written in given $N \times N$ linear system matrix form

$$A\gamma = b,$$

in which $\gamma = (\gamma_1, \gamma_2, \dots, \gamma_N)^t$ is an unknown coefficient vector that should be $b = (y_1, y_2, \dots, y_N)^t$ and the RBF interpolation matrix is given by

$$A = [\Phi_{ij}] = [\phi(\|x_i - x_j\|_2)]_{1 \leq i, j \leq N} \text{ with } \Phi_{ij} = \Phi_{ji},$$

where A is an $N \times N$, γ and b are $N \times 1$ matrices. Although, some RBFs are conditionally positive definite functions as appeared in Table 1 [15], for example, MQ, IMQ, GA, and TPS. Subsequently, polynomials are added to Eq. (4) to make sure that the resultant interpolation matrix is invertible. Such equation condition can be written as follows,

$$f(x) = \sum_{j=1}^N \gamma_j \phi(\|x - x_j\|_2) + \sum_{i=1}^M \gamma_{N+i} P_i(x) \tag{5}$$

with constraints

$$\sum_{i=1}^M \gamma_i P_i(x_j) = 0, i = 1, 2, \dots, M, \tag{6}$$

in which $P_i \in \prod_{m-1}$, $i = 1, 2, \dots, M$, where \prod_m represents the polynomial space in which the total degree of all polynomials is then m in N variables [43],

$$\binom{N+m-1}{m-1}.$$

Then, Eqs. (5) and (6) yields matrix system of $(M+N) \times (M+N)$

$$\begin{bmatrix} A & P \\ P' & o \end{bmatrix} \begin{bmatrix} \gamma \\ 0 \end{bmatrix} = \begin{bmatrix} b \\ 0 \end{bmatrix},$$

where the components of matrix A are $A = [\Phi_{i,j}] = [\phi(\|x_i - x_j\|_2)]_{1 \leq i, j \leq N}$, the components of P are $P_{i,j} = p_i[x_j]_{1 \leq i \leq N, 1 \leq j \leq M}$, and O is also $M \times M$ matrix.

Moreover, details of positive definite (PD) and conditionally positive definite (CPD) RBFs are discussed in [41, 43] and listed in Table 1. For RBFs containing the shape parameter c , such as in Table 1, small shape parameters produces more accurate results, but also associated with poorly conditioned interpolation matrix [54, 64].

Table 1. $[k]$ denotes the nearest integers less than or equal to k , and N the natural number, c a positive constant which is known as the shape parameter, and CPD denotes the m -order conditionally positive definite functions [7, 22].

Name of RBF	Definition	CPD order (m)
Multiquadrics (MQ)	$\phi(r, c) = (r^2+c)^k$ if $k > 0, k \notin N$	$[k]+1$
Inverse Multiquadrics (IMQ)	$\phi(r, c) = (r^2+c)^{-k}$ if $k > 0, k \notin N$	0
Gaussian (GA)	$\phi(r, c) = \exp\left(\frac{-r^2}{c}\right)$	0
Polyharmonic Splines (PS)	$\phi(r) = \begin{cases} r^{2k-1} & \text{if } k \in N \\ r^{2k-1} \ln r & \text{if } k \notin N \end{cases}$	$\left[\frac{k}{2}\right] + 1$
Thin Splines Plates (TPS)	$\phi(r) = (r^2) \ln r$	0

3. A NEW TOTAL VARIATION METHOD FOR MULTIPLICATIVE NOISE REMOVAL (M1)

Y. M. Huang, M. K. Ng, and Y. W. Wen (HMW) proposed the model in 2009 [30] for image restoration from given noisy image having multiplicative noise having TV regularization. In this model the authors consider a new variable $z = \log(u)$ where, $S(\Omega) = \{u \in BV(\Omega) : u > 0\}$. The minimization approach of the model (1) by [30] is formulated as:

$$\min_z \sum_{i=1}^{n^2} [z]_i + [f]_i e^{[z]_i} + \lambda \|z\|_{TV, \varepsilon}, \tag{7}$$

where $[z]_i$ is positive, negative, or zero and the corresponding $[z]_i = e^{[z]_i}$ is positive. The authors then used the unconstrained TV approach to solve the minimization functional (7) which is given as follows:

$$\min_z \left\{ \sum_{i=1}^{n^2} \left([z]_i + [f]_i e^{-[z]_i} \right) + \gamma_1 \|z - w\|_2^2 + \gamma_2 TV(w) \right\}, \tag{8}$$

where γ_1 and γ_2 is the original corrupted image, also $\|z - w\|_2^2$ represents the new fitting term, and $TV(w)$ is the total variation of w .

The above Eq. (8) leads to the following minimization algorithms by alternating minimization algorithm:

$$z^{(n)} = \arg \min_z \sum_{i=1}^{n^2} \left([z]_i + [f]_i e^{-[z]_i} \right) + \gamma_1 \|z - w^{(n-1)}\|_2^2, \tag{9}$$

$$w^{(n)} = \arg \min_w \left\{ \gamma_1 \|z^{(n)} - w\|_2^2 + TV(w) \right\}. \tag{10}$$

The associated Euler-Lagrange Eq. (9) of z - *subproblem*:

$$1 - [f]_i e^{-[z]_i} + 2\gamma_1 ([z]_i - [w^{(n-1)}]_i) = 0, \quad i = 1, 2, \dots, n^2 \tag{11}$$

was solved by the Newton method. The solution of z by Chambolle projection algorithm is utilized in the restoration problem (9) [30]. At that point, the reconstructed image for u is computed by $\exp(w)$. The rules for stopping criteria and the assurance of the two regularization parameters γ_1 and γ_2 for this model are also examined in [30].

4. PROPOSED METHOD (M2)

Since the multiplicative noise removal model (1) is

$$f = u \eta_1. \tag{12}$$

The logarithmic amplification changes [56] Eq. (12) into traditional additive noise form:

$$\log(f) = \log(u) + \log(\eta_1). \tag{13}$$

The above expression can be re-written as

$$u_0 = u + \eta \text{ or } z_{\alpha_1}^0 = g_{\alpha_1} + \eta_{\alpha_1} \text{ for all } \alpha_1 \in \Omega. \tag{14}$$

Here, we can accept η to be additive noise and can apply the traditional additive noise superposition procedure, for example, DTV filtering.

In this section, our point is to present a new methodology by utilizing digital total variation (DTV) filter alongside with radial basis functions (RBFs) to reestablish the clean image g from degraded image z in the model (14). Let $\{\alpha_j\}_{j=1}^{N_c}$ be N_c centers in $\Omega \subseteq R^2$. Here the pixels vertices are represented by $\alpha_1, \alpha_2, \dots$. The notation $\alpha_1 \sim \alpha_2$ shows that α_1 and α_2 are neighbors. All the neighbors of α_1 are denoted by

$$N_{\alpha_1} = \{ \alpha_2 \in \Omega / \alpha_2 \sim \alpha_1 \} \text{ for } \alpha_1 \sim \alpha_2 \cong \alpha_2 \sim \alpha_1.$$

Suppose $\{x_i\}_{i=1}^N$ is the distant evaluation points in $\Omega \subseteq R^2$. So for any RBF the following equations satisfied. $\phi(r) = \|r\|_2$ in R^2 , *i.e.*, $r = (x, y)$, and for $\{\alpha_j\}_{j=1}^{N_c}$. Given N_c centers, the radial basis function without polynomial term can be written as

$$s(x) = \sum_{j=1}^{N_c} \rho_j \phi(\|x - x_j\|_2), \quad (15)$$

where ρ_i coefficients in RBF are determined via enforcing the interpolation condition

$$s(x_j) = z^0,$$

a set of points that usually coincides with N_c centers. The interpolation condition at N_c centers results in an $N_c \times N_c$ linear system

$$A\rho = z^0.$$

The solution of the above system results in the solution for expansion coefficients of ρ , where $\rho = (\rho_1, \rho_2, \dots, \rho_{N_c})^t$ and $z^0 = (z_1^0, z_2^0, \dots, z_{N_c}^0)^t$. The matrix A is called interpolation matrix or system matrix and is given by

$$A = [\Phi_{i,j}] = [\phi(\|x_i - \alpha_j\|_2)]_{1 \leq i, j \leq N_c}.$$

This system matrix A is always invertible because it is always positive definite matrix [43, 49]. Hence we have

$$\rho = A^{-1}z^0. \quad (16)$$

The interpolant is evaluated using Eq. (15) at N evaluation points $\{x_i\}_{i=1}^N$, through forming $N \times N_c$ evaluation matrix B which is given as

$$B = [\Phi_{i,j}] = [\phi(\|x_i - \alpha_j\|_2)]_{1 \leq i \leq N, j \leq N_c}.$$

The interpolant is then evaluated at N points using matrix-vector product to produce g as follows,

$$g = B\rho. \quad (17)$$

Using Eqs. (16) and (17) the following equation is obtained.

$$g = BA^{-1}z^0$$

or

$$g = Hz^0 \text{ where } H = BA^{-1}, \quad (18)$$

which gives an approximate solution at any point in Ω .

As the minimization approach for model (14) utilizing DTV method [10] is given as

$$\min_g E(g) = \sum_{\alpha_1 \in \Omega} \|\nabla_p g_{\alpha_1}\|_a + \frac{\lambda}{2} \|g_{\alpha_1} - z_{\alpha_1}^0\|_{\Omega}^2 \text{ for all } \alpha_1 \in \Omega, \tag{19}$$

where the first term is the regularized local variation of g , the second term is called data fidelity term and λ is the fitting parameter and a is regularized parameter. The corresponding restoration equation [10] of Eq. (19) is given as

$$0 = \sum_{\alpha_2 \in N_{\alpha_1}} (g_{\alpha_1} - g_{\alpha_2}) w_{\alpha_1 \alpha_2}(g) + \lambda (g_{\alpha_1} - z_{\alpha_1}^0), \tag{20}$$

where

$$w_{\alpha_1 \alpha_2} = \frac{1}{\|\nabla_p g_{\alpha_1}\|_a} + \frac{1}{\|\nabla_p g_{\alpha_2}\|_a}, \tag{21}$$

$$\|\nabla_p g_{\alpha_1}\| := \sqrt{a^2 + \sum_{\alpha_2 \sim \alpha_1} (g_{\alpha_2} - g_{\alpha_1})},$$

and

$$\|\nabla_p g_{\alpha_1}\| := \sqrt{a^2 + \|\nabla_p g_{\alpha_1}\|}, \tag{22}$$

for small fixed value of a , i.e., $a = 10^{-4}$. Therefore Eq. (20) can be fixed and re-written as follow

$$0 = \sum_{\alpha_2 \sim \alpha_1} (g_{\alpha_2} - g_{\alpha_1}) \left(\frac{1}{\|\nabla_p g_{\alpha_1}\|_a} + \frac{1}{\|\nabla_p g_{\alpha_2}\|_a} \right) + \lambda (g_{\alpha_1} - z_{\alpha_1}^0). \tag{23}$$

In order to get the faster steady state restoration solution, the steady state time marching equation is derived from Eq. (23) as inspired by the recent work of Marquina and Osher [42] and is denoted by the equation below.

$$\frac{dg_{\alpha_1}}{dt} = \sum_{\alpha_2 \sim \alpha_1} (g_{\alpha_2} - g_{\alpha_1}) \left(\frac{1}{\|\nabla_p g_{\alpha_1}\|_a} + \frac{1}{\|\nabla_p g_{\alpha_2}\|_a} \right) + \lambda \|\nabla_p g_{\alpha_1}\|_a (g_{\alpha_1} - z_{\alpha_1}^0), \tag{24}$$

or

$$\frac{dg_{\alpha_1}}{dt} = \sum_{\alpha_2 \sim \alpha_1} (g_{\alpha_2} - g_{\alpha_1}) w_{\alpha_1 \alpha_2} + \lambda \|\nabla_p g_{\alpha_1}\|_a (g_{\alpha_1} - z_{\alpha_1}^0). \tag{25}$$

Combining the restoration Eq. (25) with Eq. (18), and solve the resultant restoration equation by collocation method (Kansa method). We use the Gauss-Jacobi iterative method to solve the nonlinear system of restoration equations as follow,

$$g_{\alpha_1}^{(n+1)} = g_{\alpha_1}^{(n)} + dt \left[\sum_{\alpha_2 \sim \alpha_1} w_{\alpha_1 \alpha_2} (g^{(n)}) (g_{\alpha_2}^{(n)} - g_{\alpha_1}^{(n)}) - \lambda \left(\sum_{\alpha_2 \sim \alpha_1} (g_{\alpha_2}^{(n)} - g_{\alpha_1}^{(n)}) \right)^{\frac{1}{2}} (g_{\alpha_1}^{(n)} - z_{\alpha_1}^{(0)}) \right] \tag{26}$$

with $z_{\alpha_1}^{(0)} = z_{\alpha_1}^0$, $g_{\alpha_1} = H_{\alpha_1} z^0 = B_{\alpha_1} A^{-1} z^0$, and $g_{\alpha_2} = H_{\alpha_2} z^0 = B_{\alpha_2} A^{-1} z^0$. Where

$$B_{\alpha_1} = [\Phi_{\alpha_1,j}] = [\phi(\|x\alpha_1 - \alpha_j\|_2)] \text{ for } i = 1, 2, \dots, Nc$$

and

$$B_{\alpha_2} = [\Phi_{\alpha_2,j}] = [\phi(\|x\alpha_2 - \alpha_j\|_2)] \text{ for } i = 1, 2, \dots, Nc.$$

Here, g_{α_1} and g_{α_2} are the approximate values at vertices α_1 and α_2 respectively.

As the Kansa technique in RBF does not necessarily to satisfy the obtained non-linear system of Eq. (26), so we have more flexibility to choose an RBF. The well-known RBF in the Kansa method is the multiquadric (MQ) [34, 41], which usually shows spectral accuracy if a suitable shape parameter c is chosen. Here, the shape parameter c used in RBF is also one of the most important parameters for the smoothness in our method M2. For the proper values of c , our proposed method produces more accurate and smooth results in image restoration having multiplicative noise. In this method, the shape parameter c and fitting parameter λ are the two critical parameters for the smooth result, and its optimal values rely upon the size of the image and the noise level in the image. On the other hand, the regularization parameter a is used to avoid a zero, so its value is usually taken $a = 10^{-4}$. Where z_{α_1} shows the value at any pixel α_1 . The locality and adaptivity for smooth results by DTV filtering have already been discussed in [10] for the smooth solution.

Algorithm for proposed model M2:

RBF:

1. Initialize the values of λ , ε , c , and z^0 .
2. Set the centers $\alpha_1, \alpha_2, \dots, \alpha_{|\Omega|}$.
3. Find the σ according to Eq. (16) by MQ-RBF.
4. Find g according to Eq. (18) by MQ-RBF.

DTV filtering:

5. Set the centers $\alpha_1 \leq \alpha_2 \leq \alpha_{|\Omega|}$, set $n = 0$.
6. $n = n + 1$. For each center point α_1 and all its neighbors α_2 calculate the local variation $\|\nabla_p g_{\alpha_1}\|$ and the weighted function $w_{\alpha_1 \alpha_2}(g^{(n)})$ according to Eqs. (22) and (21).
7. Put $w_{\alpha_1 \alpha_2}(g^{(n)})$ and $g_{\alpha_1}^{(n)}$ as MQ-RBF in Eq. (26) to get $N \times Nc$ nonlinear system of equations.
8. For each α_1 , compute $g_{\alpha_1}^{(n+1)}$ according to Eq. (26) by RBF approximation.

Where we choose $z^{(0)} = z^0$.

9. $\frac{\|g^{(n+1)} - g^{(n)}\|}{\|g^{(n)}\|} < \varepsilon = 10^{-5}$ (stopping criteria), go to step 11.
 10. Go to step 6.
 11. End.
 12. Output $g = g_{\alpha_1}^{(n+1)}$.
-

5. EXPERIMENTAL RESULTS AND DISCUSSION

In this section, some numerical results are provided to demonstrate the performance of our proposed method M2 in comparison with the results of method M1. The test images are “Lena”, “BMW”, “SynImage1”, “SynImage2”, “Cameraman”, “SynImage3”, “SynImage4”, and “Shape2” which are shown in Fig. 1. We test our images on two sorts of multiplicative noises, *i.e.*, multiplicative noise (Gamma distribution) with mean value 1 and variance L_1 and speckle noise (Gamma distribution) with mean value 1 and variance L_2 .

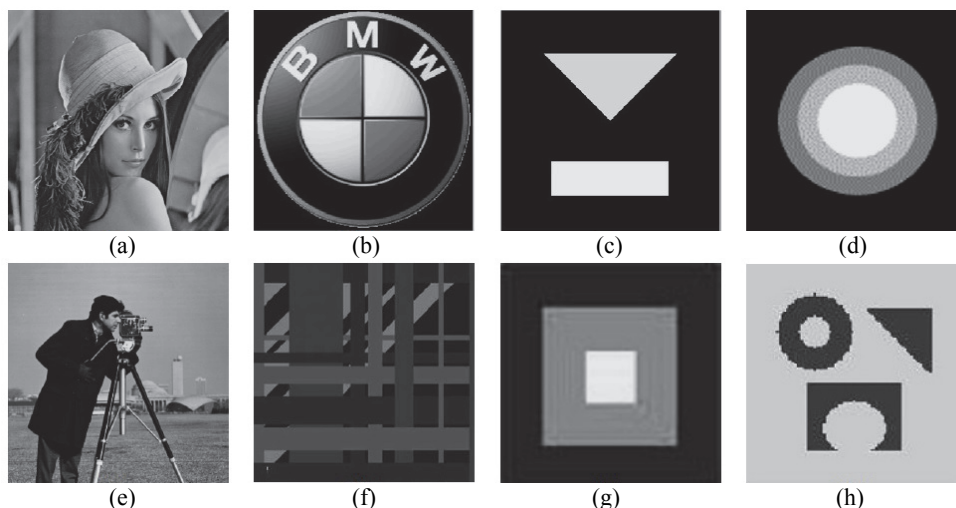


Fig. 1. Test images in our experiments (a) Lena; (b) BMW; (c) SynImage1; (d) SynImage2; (e) Cameraman; (f) SynImage3; (g) SynImage4; (h) Shape2.

For the 2D case, there are many ways to define N_α for proposed model M2. One way is to consider a p point neighbor of a node α as consisting of all p points that are closest to α . In this paper, N_α is defined in the best way. Dividing the region surrounding a point α into p regions of equal angles N_α is defined such that it consists of points in each region that are closest to α as discussed in [10]. Here, it is assumed that $p =$ the size of the image, for the sake of comparison between two models; M1 and M2. Multiquadric radial basis function (MQ-RBF) is utilized for the proposed method M2. For the comparison of image restoration results, the peak-signal-to-noise ratio (PSNR) is considered. This measure has been commonly used and applied to determine the quality of restore image. The following formula can calculate it.

$$PSNR = 10 \times \log_{10} \left[\frac{M \times N \max \{ \tilde{u} \}}{\| \tilde{u} - u \|} \right] \quad (27)$$

Where \tilde{u} is the given image, u is the restored image and $M \times N$ is the size of the image.

Signal-to-noise ratio (SNR) has also used to find the visual quality of the restoration of the restored image. It can be deafened as

$$SNR = 10 \times \log_{10} \frac{\|u - u_0\|}{\|n - n_0\|}, \quad (28)$$

where u and n denote the true image and noise, u_0 and n_0 represent their mean values in the image domain Ω . Again greater the SNR value, better will be the restoration result.

Iterations in our algorithm are terminated when the following condition is satisfied.

$$\frac{\|u^{(k+1)} - u^{(k)}\|}{\|u^{(k)}\|} < \varepsilon, \quad (29)$$

where ε indicates the maximum permissible error. Here, it is set to be 10^{-5} .

Here we use the Multiquadric (MQ) RBF to test and compare the results of model M2 with model M1. For each point (x_j, y_j) , MQ-RBF is defined as equation below.

$$\phi_j(x, y) = \sqrt{c^2 + r_j^2} = \sqrt{c^2 + ((x - x_j)^2 + (y - y_j)^2)},$$

where $r_j = \sqrt{(x - x_j)^2 + (y - y_j)^2}$.

Test 1:

In this first test, the two methods, M1, and M2 are applied and tested on natural images ‘‘Lena’’ and ‘‘BMW’’ with multiplicative noise (Gama noise) with noise levels $L_1 = 10$ and $L_1 = 12$, respectively, which are shown in the Figs. 2 and 3, respectively. In all two Figures, (a) and (b) are the original and noisy images while (c) and (d) depict the restored images by the methods M1 and M2, respectively. In each case, we can see that the quality of the restorations of two the images by proposed method M2 are quite efficient than method M1. In model M1, the restoration quality of the pictures is good but creates the staircase effect, which is a congenital disability of TV regularization method. These reconstructed images are shown in the Figs. 2 (c) and 3 (c), respectively. In our technique M2, the visual quality and preservation of edges of the restored images are far superior to method M1 because of edge detective property of DTV filter and the meshless characteristics of MQ-RBF used in M2. These denoised images are shown in the Figs. 2 (d) and 3 (d), respectively. In M2, the shape parameter c plays a vital role in image denoising. The range of optimal values of shape parameter for M2 in this test is set to $1.68 \leq c \leq 1.75$. Moreover, the PSNR values for the two images ‘‘Lena’’ and ‘‘Bmw’’ for two methods M1 and M2 are listed in Table 2. The bigger the PSNR value, the better the denoising performance. It can be verified from Table 2 that the PSNR values of method M2 are greater than model M1 for the two images, which shows the dynamic restoration performance of the M2 over M1. The number of iterations and CPU time of computation required for convergence of the two methods M1 and M2 are also listed in Table 2. It can likewise be seen from the Table 2 that the number of iterations and CPU

time of computation of the M2 are smaller than M1, which indicates the faster restoration performance of M2 over M1 due to MQ-RBF properties used in M2. The best optimal values of parameters of our technique M2 (shape parameter (c)), fitting parameter (λ) for the two images “Lena” and “BMW” are (1.74, 0.113) and (1.69, 0.211), respectively. So, it is evident from this test, that the performance of our mesh-free method M2 is superior to that of mesh-based model M1 regarding visual restoration quality (PSNR), the number of iterations and CPU time of computation. In this test we select $dt = 0.001$.



Fig. 2. Experimental results on “Lena” images; (a) True image; (b) Degrade image with $L_1 = 10$; (c) Obtained image by method M1; (d) Obtained image by method M2.

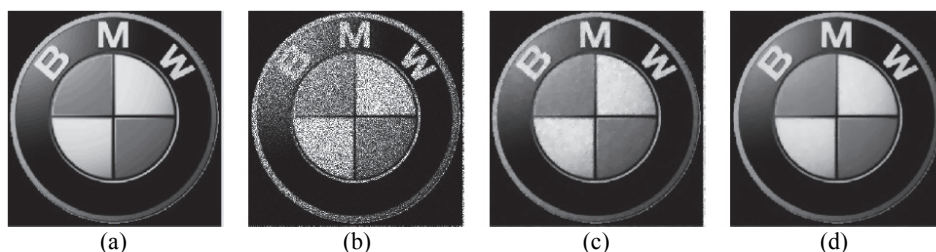


Fig. 3. Experimental results on “BMW” images; (a) Noiseless image; (b) Degrade image with $L_1 = 12$; (c) Restored image by method M1; (d) Restored image by method M2.

Test 2:

In this second test, we study how our algorithm M2 deals with the synthetic images “SynImage1” and “SynImage2” having the speckle noise (Gama noise) which are shown in the Figs. 4 and 5, respectively. The noise level for the two artificial images “SynImage1” and “SynImage2” in this test are $L_2 = 10$ and $L_2 = 12$, respectively. In both cases, the restoration results by M2 are better than M1. In M1, we obtain better-restored images but have staircase effect due to TV regularization and the problem with the initial guess of the algorithm used in method M1. These restored images by M1 can be seen in Figs. 4 (c) and 5 (c). In this test, our proposed method M2 shows the improved performance regarding the visual quality of the restoration (PSNR), edges preservation of images than M1 because of the built-in edge detect the property of DTV method and mesh-free characteristics of MQ-RBF approximations used in M2. These resultant images are shown in Figs. 4 (d) and 5 (d). In approach M2, the shape parameter c plays a significant role in image denoising. The range for the optimal values of c for M2 in this example is set to $1.77 \leq c \leq 1.84$. In this case, the parameters used for the two images “SynImage1” and “SynImage2” for the method M2 (shape parameter (c), fitting parameter (λ)) are (1.83,

0.011) and (1.78, 0.021) respectively. We also choose $dt = 0.001$. The preference of the two methods M1 and M2 concerning restoration (PSNR values), CPU computation time and the number of iterations required for convergence for the two images, *i.e.*, “SynImage1” and “SynImage2”, can be seen in Table 2. Again, from Table 2, M2 shows superior and faster performance than M1.

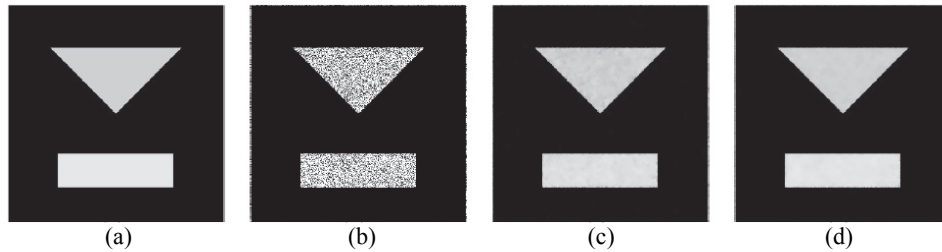


Fig. 4. Test results on “SynImage1” images; (a) Original image; (b) Noisy image with $L_2 = 10$; (c) De-noised image by method M1; (d) De-noised image by method M2.

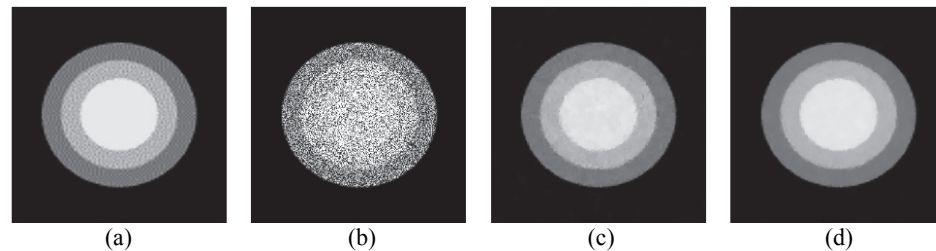


Fig. 5. Test results on “SynImage2” images; (a) Original image; (b) Degrade image with $L_2 = 12$; (c) Restored image by method M1; (d) Restored image by method M2.

Table 2. Comparison of model M1 and model M2 regarding PSNR, number of iterations and CPU-time (in seconds).

Image	Size	Model M1			Model M2		
		PSNR	Iterations	CPU Time	PSNR	Iterations	CPU Time
Lena	300^2	27.82	118	40.75	29.08	46	22.92
Parrot	300^2	26.24	105	34.09	27.36	40	19.32
SynImage1	300^2	25.03	128	68.59	26.54	51	27.43
SynImage2	300^2	24.96	116	53.31	25.36	47	23.87

Test 3:

In this test, both the methodologies M1 and M2 are examined on “Cameraman” having different noise levels. It can be noticed that the quality of image restoration (PSNR) of the proposed method M2 is better than M1 due to the properties of MQ-RBF used in M2 mainly when the noise variance is large. These results are given in Figs. 6-8, and Table 3. The values of the parameters for M2 (shape parameter (c), fitting parameter (λ)) for the three different noise levels *i.e.*, $L_2 = 5, 7, 9$ for “Cameraman” are (1.73, 0.110), (1.76, 0.152), and (1.78, 0.189) respectively. In this case we select $dt = 0.001$.

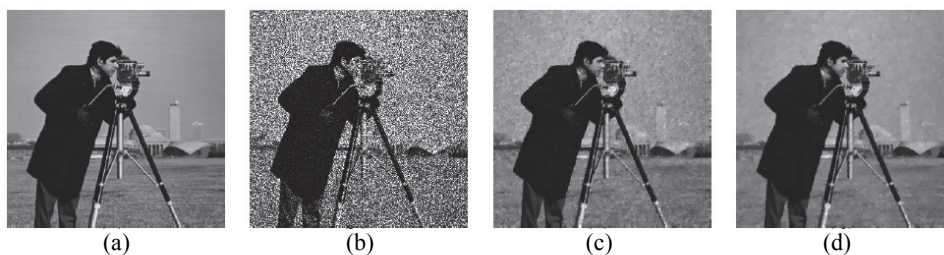


Fig. 6. Experimental results on “Cameraman” image; (a) True image; (b) Degrade image with $L_2 = 5$; (c) Processed with method M1; (d) Processed with method M2.

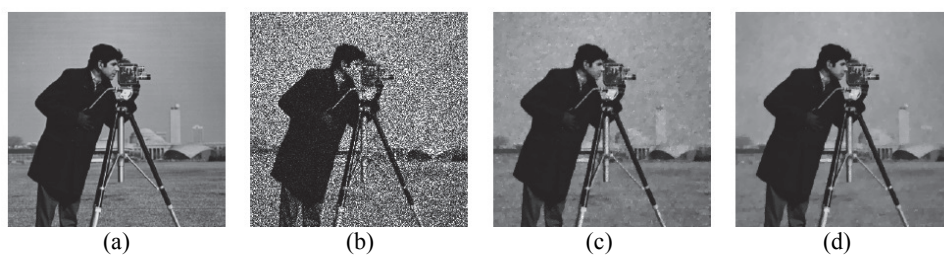


Fig. 7. Experimental results on “Cameraman” image; (a) Original image; (b) Noisy image with $L_2 = 7$; (c) Reconstructed image by method M1; (d) Reconstructed image by method M2.

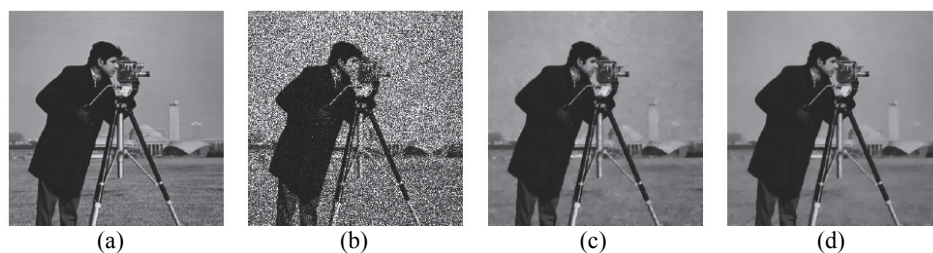


Fig. 8. Experimental results on “Cameraman” image; (a) Original image; (b) Degrade image with $L_2 = 9$; (c) Restored image by method M1; (d) Restored image by method M2.

Table 3. Comparison of PSNR value of the restored image “Cameraman” for different speckle noise values for two methods M1 and M2.

Image	$L_1 = 5$		$L_1 = 7$		$L_1 = 9$	
	M1	M2	M1	M2	M1	M2
Cameraman	23.46	25.22	24.89	26.02	25.91	27.04

Test 4:

Here, the homogeneity is checked, and loss (or preservation) is examined for the two techniques M1 and M2 while being applied to “Lena”. For this purpose, different lines of the original image compared with noisy and restored images that are shown in Figs. 9 and 10. It is clear that the lines restored by proposed method M2 (shown in Figs. 9 (c) and 10 (c)) is far better than what acquired utilizing model M1 that are presented in the Figs. 9 (b) and 10 (b).

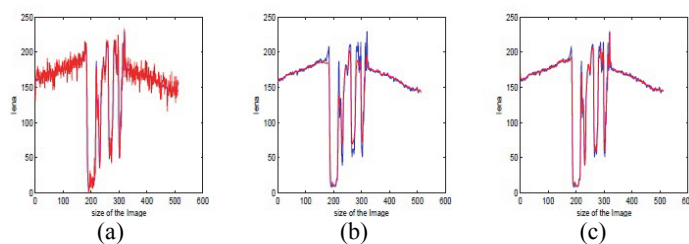


Fig. 9. The 129th line compression of the original image with noisy image, restored image by method M1, and restored the image by model M2 of the “Lena”; (a) Original and noisy images lines; (b) Original and restored by method M1 images lines; (c) Original and restored by method M2 images lines. Here the blue line is the original image, and the red line is the restored image.

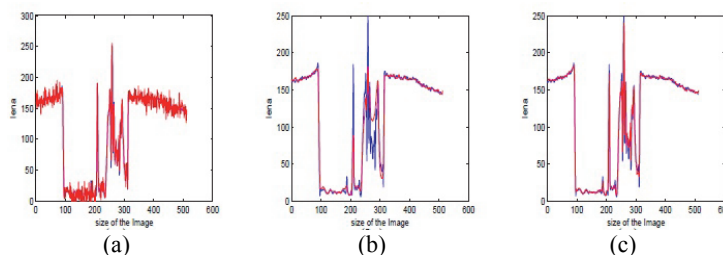


Fig. 10. The 178th line compression of the original image with noisy image, restored image by method M1, and restored the image by model M2 of the “Lena”; (a) Original and noisy images lines; (b) Original and restored by method M1 images lines; (c) Original and restored by method M2 images lines. Here the blue line is the original image, and the red line is the restored image.

5.1 Shape Parameter Analysis

In this subsection, we compare the quality of restoration (PSNR) of the restored images by choosing different values of shape parameter c for “Lena” and “SynImage2” having multiplicative and speckle noises as mentioned in Tests 1 and 2, respectively. Different values of the shape parameter c affect the image restoration quality (PSNR) of two images “Lena” and “SynImage2,” that are shown in Figs. 11 and 12. The PSNR values of the two images are also given in Table 4 for different values of shape parameter.



Fig. 11. Experimental results on Lena; (a) Original image; (b) Noisy image with $L_1 = 10$; (c) Resultant image by optimal value of $c = 1.74$; (d) Resultant image by $c = 1.88$; (e) Resultant image by $c = 1.69$.

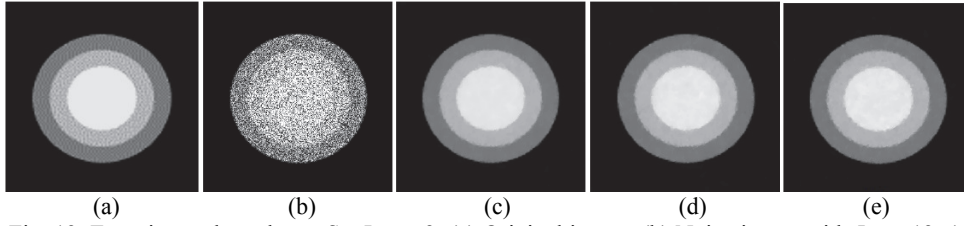


Fig. 12. Experimental results on SynImage2; (a) Original image; (b) Noisy image with $L_{12} = 12$; (c) Obtained image by optimal value of $c = 1.78$; (d) Obtained image by $c = 1.82$; (e) Obtained image by $c = 1.71$.

Table 4. Comparison of the image quantity (PSNR) for different values (increase and decrease) in shape parameter c with the optimal value of shape parameter c of the proposed method M2 for two images.

Image	Size	Optimal value c	PSNR	Increase c	PSNR	Decrease c	PSNR
Lena	300^2	1.74	29.08	1.88	28.20	1.69	27.39
SynImage2	300^2	1.78	25.36	1.82	25.10	1.71	24.96

6. COMPARISON WITH OTHERS METHODS

Here, we have also compared our method M2 with some other variational methods used for multiplicative noise removal problems.

RLO method:

The RLO-model is presented in [50], and its solution is also discussed in [50], which is given by the following gradient projection iterative scheme:

$$u^{(n+1)} = u^{(n)} + dt \left[D_x^- \left(\frac{D_x^+ u^{(n)}}{|D_x^+ u^{(n)}|_\varepsilon} \right) + D_y^- \left(\frac{D_y^+ u^{(n)}}{|D_y^+ u^{(n)}|_\varepsilon} \right) + \lambda_1 \frac{f^2}{(u^{(n)} + \varepsilon)^3} + \mu \frac{f}{(u^{(n)} + \varepsilon)^2} \right]. \quad (30)$$

The experimental values of the two Lagrange multipliers $\lambda_1, \mu, \varepsilon$ and time step dt are already discussed and explained in [50].

AA method:

This model is also presented and described in [3], its solution is given by gradient projection method:

$$u^{(n+1)} = u^{(n)} + dt \left[\lambda_2 \left(D_x^- \left(\frac{D_x^+ u^{(n)}}{|D_x^+ u^{(n)}|_\varepsilon} \right) + D_y^- \left(\frac{D_y^+ u^{(n)}}{|D_y^+ u^{(n)}|_\varepsilon} \right) \right) + \frac{f}{(u^{(n)} + \varepsilon)^2} \right]. \quad (31)$$

The optimal values of ε and dt are taken as RLO method and Lagrange multiplier λ_2 is discussed in [3].

LL method:

This method was presented by Huang *et al.* in [28] for image restoration having

multiplicative noise which is given as follow;

$$\tilde{u} = \arg \min_u E(u) = \int_{\Omega} \left(\beta_1 + \frac{u}{\beta_2} \right) |\nabla u| dx dy + \int_{\Omega} \left(\log(u) + \frac{f}{u} \right) dx dy,$$

where

$$|\nabla u| = \sqrt{u_x^2 + u_y^2}. \quad (32)$$

In the above Eq. (32), the first term is regularization term while the second term is fitting/fidelity term and β_1 and β_2 are two fitting parameters. The corresponding Euler-Lagrange equation is given as under;

$$-\nabla \cdot \left[\frac{\nabla u}{|\nabla u|^2 + \beta} \right] + \tilde{\lambda}(u - f) = 0 \text{ in } \Omega \text{ for } t > 0, (x, y) \in R, \quad (33)$$

where $\tilde{\lambda} = \frac{1}{u(\beta_1 + \beta_2)}$. The gradient descent is applied to solve Eq. (33). For further details, see [28].

In our computational experiments, we use $u^{(0)} = f$ as the initial guess for RLO and AA models.

Here, ROL, AA, and LL methods are compared with proposed method M2 for the same images having the same size and noise variances and same parameter values that have been selected in [28]. Again, from the results in Figs. 13 and 14, and Table 5, we can observe that our proposed technique M2 has better performance in the visual quality of restoration (PSNR), iterations and CPU times compared to ROL, AA and LL methods. The values of the parameters selected for our proposed model M2 (shape parameter (c), fitting parameter (λ) for the two images ‘‘SynImage3’’ and ‘‘SynImage4’’ are (1.87, 0.033) and (1.86, 0.029) respectively.

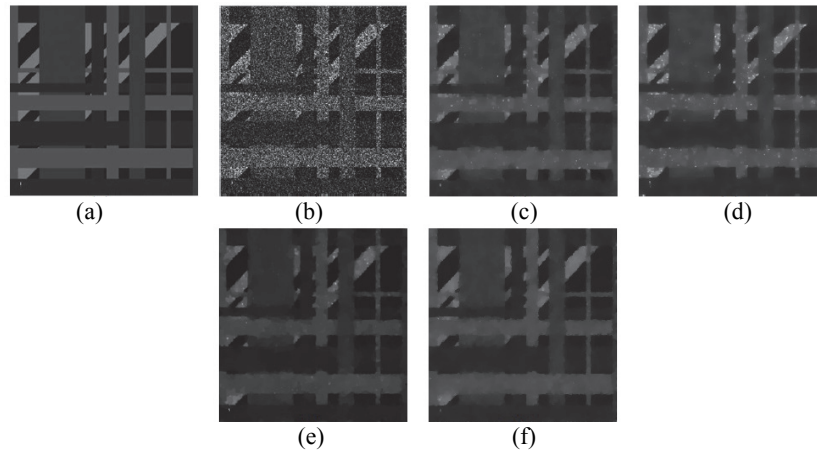


Fig. 13. Denoised results on SynImage3; (a) Original image; (b) Noisy image with speckle noise $L_2 = 2$; (c) Resultant image by RLO method; (d) Resultant image by AA method; (e) Resultant image by LL method; (f) Resultant image by our method M2.

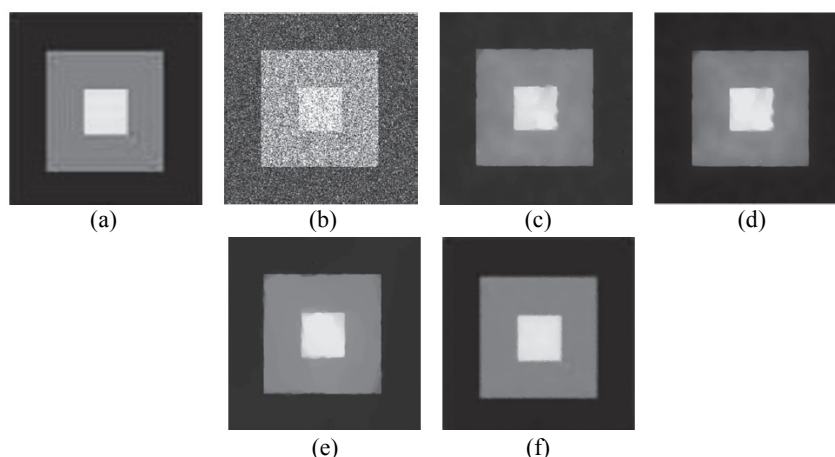


Fig. 14. Obtained results on SynImage4; (a) Original image; (b) Noisy image with speckle noise $L_2 = 5$; (c) De-noised image by RLO method; (d) De-noised image by AA method; (e) De-noised image by LL method; (f) Resultant image by our method M2.

Table 5. Comparison of models RLO, AA, LL and proposed our method M2 in terms of PSNR, number of iterations and CPU-time (in seconds) of the two artificial images of size 256^2 .

Image	RLO method			AA method			LL method			Our method M2		
	PSNR	It.	Time	PSNR	It.	Time	PSNR	It.	Time	PSNR	It.	Time
SynImage3	25.84	251	152.9	25.71	246	42.7	26.95	53	100.0	27.03	47	41.9
SynImage4	29.71	591	261.2	31.86	575	77.9	33.17	119	166.7	33.29	108	38.1

6.1 PDWAM Model

X. Wang, *et al.* [63] proposed primal-dual algorithm to solve the iteratively re-weighted TV-based (PDWAM) model [63] for multiplicative noise removal. The minimization functional of the model is

$$z_{op} = \arg \min_z \left\{ \mu \int_{\Omega} g(x)\varphi(z)dx dy + \int_{\Omega} (z - fe^{-z})dx dy \right\}, \tag{34}$$

where $z(x) = \log(u(x))$, $\varphi(z) = |\nabla z|$. μ is the regularization parameter, and $g(x)$ represents the nonnegative weight function which is defined as under:

$$g(x) = \begin{cases} 1 & n=1 \\ \frac{1}{|\nabla z^{(n-1)}(x) + \varepsilon^{(n)}|} & n \geq 2 \end{cases}, \tag{35}$$

where n is the number of outer iteration and $\varepsilon^{(n)}$ represents the stability for iterations. The authors split Eq. (34) as done in [30] as follow:

$$\min_{z,w} J(w, z) = \min_{z,w} \left\{ \int_{\Omega} (z - fe^{-z}) dx dy + \gamma \int_{\Omega} (w - z)^2 dx dy + \mu \int_{\Omega} g(x) |\nabla w| dx dy \right\}, \quad (36)$$

where w is an auxiliary function and γ is the regularization parameter which represents the relation between w and z . The authors then used the alternating minimization algorithm to split Eq. (36) into two equations, *i.e.*,

$$w^{(n)} = \arg \min_w \left\{ \gamma \int_{\Omega} (z - fe^{-z}) dx dy + \mu \int_{\Omega} g(x) |\nabla w| dx dy \right\}, \quad (37)$$

$$z^{(n)} = \arg \min_z \left\{ \int_{\Omega} (z - fe^{-z}) dx dy + \gamma \int_{\Omega} (w^{(n)} - z)^2 dx dy \right\}. \quad (38)$$

By using the primal-dual algorithm, the authors defined the convex close set K as

$$K = \overline{\left\{ \text{div} p / p \in C_c^1(\Omega, R^2), |p| \leq g(x), \forall x \in \Omega \right\}}.$$

Where $\overline{\{\cdot\}}$ denotes the convex close set of $\{\cdot\}$. So this procedure the Euler Eq. (37) is given as under:

$$w^{(n)} = z^{(n)} - \pi \frac{\mu}{2\gamma} K(z^{(n-1)}). \quad (39)$$

The nonlinear system of Eq. (38) is defined in similar way as under:

$$(1 - fe^{-z}) + 2\gamma(z - w^{(n)}) = 0. \quad (40)$$

For further details see [63].

The displayed results in Figs. 15-16, and Table 6 recommend that the proposed algorithm M2 performs superior to PDWAM regarding the quality of restoration (SNR) for the same noise levels and parameters as taken in the model [63]. The values of parameters for the two images ‘‘Shape2’’ and ‘‘Lena’’ for our method M2 (shape parameter (c) , fitting parameter (λ)) are (1.80, 0.019) and (1.74, 0.196) respectively. Here, the value of dt is selected as 0.001.

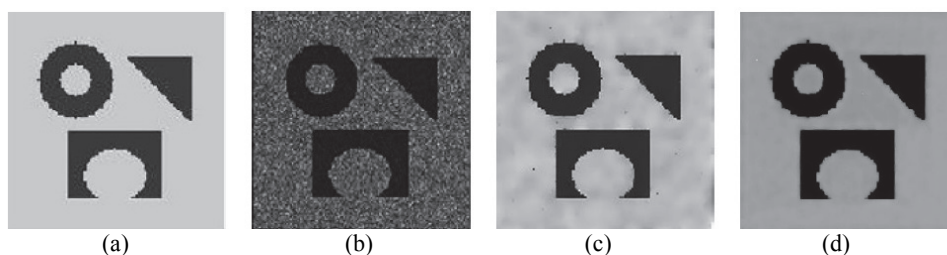


Fig. 15. Resultant results on Shape2; (a) Original image; (b) Noisy image with multiplicative noise having standard variance 1/10; (c) Restored image by PDWAM method; (d) Restored image by method M2.

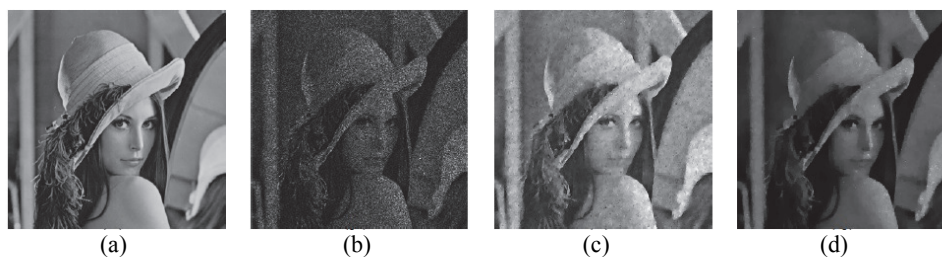


Fig. 16. Experimental results on Lena; (a) Original image; (b) Noisy image with multiplicative noise having standard variance 1/10; (c) Obtained image by PDWAM method; (d) Obtained image by method M2.

Table 6. Comparison of PDWAM and our method M2 regarding of SNR.

Image	Size	PDWAM	Our proposed method M2
		SNR	SNR
Shape2	256 ²	16.0540	16.9501
Lena	256 ²	10.9022	12.3270

7. SENSITIVITY ANALYSIS OF PARAMETERS

To discuss the selection of the shape parameter (c) and fitting parameter (λ) used in our proposed method M2. It is suggested from our experience that all the two parameters c and λ are harder to pick. In any case, their ideal values are adjusted and tuned according to the noise variance, image size, *etc.* It has been observed that the range of values allowed is: $c \in [1.68, 1.84]$ and $\lambda \in [0.0083, 0.3160]$, for natural and synthetic images according to the noise variance $L_1 = 10, 12$ and $L_2 = 10, 12$ respectively. It demonstrates that all the parameters c and λ are more imperative for enhancing de-noising performance. Similarly, the number of iterations needed for convergence is considered to be in the range [34, 37] for results with enhanced PSNR. Thus, the accessibility of data about the instability of the de-noising effect on the user-chosen parameters is helpful to keep away from wrong choices. For brevity, for Tables 7 and 8 we shall denote by

- $(\cdot)\%$ increase $-\uparrow$ and $(\cdot)\%$ decrease $-\downarrow$.
- For example $(0.15)\downarrow$ stands for 0.15% the decrease in PSNR.
- $(0.22)\uparrow$ stands for 0.22% increase in PSNR.

Table 7. PSNR value of the reestablished picture “Lena” with ideal values of c and λ is 29.08. Parameter sensitivity examination for our proposed technique M2 by percentage increased in values of the parameters c and λ values, with the resultant percentage increase or decrease in PSNR of the restored image of size (300^2) .

Image	40%(\uparrow)			70%(\uparrow)		
	c	λ	PSNR	c	λ	PSNR
Lena	2.44	0.1582	2.38(\downarrow)	2.96	0.1921	4.21(\downarrow)

Table 8. PSNR value of the reestablished picture “Lena” with ideal values of c and λ is 29.08. Parameter sensitivity examination for our proposed technique M2 by percentage decreased in values of the parameters c and λ values, with the resultant percentage increase or decrease in PSNR of the restored image of size (300^2) .

Image	40%(↑)			70%(↑)		
	c	λ	PSNR	c	λ	PSNR
Lena	1.04	0.0678	2.69(↓)	0.52	0.0339	5.15(↓)

8. CONCLUSION

In this paper, a new DTV based mesh-free algorithm for multiplicative noise removal is presented in which DTV filter is employed in conjunction with MQ-RBF approximation. This algorithm is exploited for the solution of non-linear equation arisen from the minimization of the associated DTV functional. The proposed methodology based on the Kansa method is mathematically robust and straightforward compared with the classical mesh-based method and hence provides more optimal results because of its mesh-free merit. The significant advantage of the present strategy is that it not only restores the images but also allows smooth translation without sacrificing sharp edges.

This approach is tested on different artificial and real images for multiplicative noise, and the results are compared with the current model. Our experimental results have demonstrated that the quality of the restoration of images, the number of iterations, and the CPU times with the use of the proposed method is excellent, and the proposed method is efficient. We have additionally seen that the execution of our proposed technique is apparently better than that of the current method regarding restoration quality (PSNR and SNR), the number of iterations, and CPU times on account of the mesh-free properties of RBF utilized in our technique. The choice of shape parameter $\$c\$$ also plays an essential role in our algorithm, which affects the image restoration. The analysis of shape parameter and sensitivity of parameters have also been discussed. A comparison with other related methods is also presented.

However, this technique results in an unsymmetrical interpolation matrix. Also, sometimes, this algorithm suffers relatively lower accuracy in boundary-adjacent regions. These problems are under intense study and results will be reported in the subsequent paper.

ACKNOWLEDGMENT

The work described in this paper was supported by the National Natural Science Foundation of China (No. 11702083), the Natural Science Foundation of Jiangsu Province (No. BK20150795), the Fundamental Research Funds for the Central Universities (No. 2018B16714), and the State Key Laboratory of Mechanics and Control of Mechanical Structures (Nanjing University of Aeronautics and Astronautics) (No. MCMS-0218 G01).

REFERENCES

1. A. Achim, P. Tsakalides, and A. Bezerianos, "SAR image denoising via bayesian wavelet shrinkage based on heavy-tailed modeling," *IEEE Transactions on Geoscience and Remote Sensing*, Vol. 41, 2003, pp. 1773-1784.
2. G. Anastassiou, S. Osher, and J. Shen, *Handbook of Analytic Computational Methods in Applied Mathematics*, E-publishing, Chapman and Hall/CRC, 2000, pp. 751-769.
3. G. Aubert and Z. F. O. Aujol, "A variational approach to removing multiplicative noise," *SIAM Journal on Applied Mathematics*, Vol. 68, 2008, pp. 925-946.
4. A. Beck and M. Teboulle, "A fast iterative shrinkage-thresholding algorithm for linear inverse problems," *SIAM Journal on Imaging Sciences*, Vol. 2, 2009, pp. 183-202.
5. J. Biazer and M. Hosami, "An interval for the shape parameter in radial basis function approximation," *Applied Mathematics and Computation*, Vol. 315, 2017, pp. 131-149.
6. J. M. Bioucas-Dias and M. A. T. Figueiredo, "Multiplicative noise removal using variable splitting and constrained optimization," *IEEE Transactions on Image Processing*, Vol. 19, 2010, pp. 1720-1730.
7. M. D. Buhmann, *Radial Basis Functions: Theory and Implementations*, 1st ed., Cambridge University Press, UK, 2003.
8. A. Burgel, T. Grahls, and T. Sonar, "From continuous recovery to discrete filtering in numerical approximations of conservation laws," *Applied Numerical Mathematics*, Vol. 42, 2002, pp. 47-60.
9. A. Burger and T. Sonar, "Discrete filtering of the numerical solution of hyperbolic conservation laws," *International Journal for Numerical Methods in Fluids*, Vol. 40, 2002, pp. 263-271.
10. T. F. Chan, S. Osher, and J. Shen, "The digital TV filter and nonlinear denoising," *IEEE Transactions on Image Processing*, Vol. 10, 2001, pp. 231-241.
11. D. Q. Chen, "Regularized generalized inverse linearized accelerating minimization algorithm for frame-based poissonian image deblurring," *SIAM Journal on Imaging Sciences*, Vol. 7, 2014, pp. 716-739.
12. D. Q. Chen and Y. Zhou, "Multiplicative denoising based on linearized alternating direction method using discrepancy function constraint," *Journal of Scientific Computing*, Vol. 60, 2014, pp. 483-504.
13. D. Q. Chen and L. Z. Chen, "Deconvolving poissonian images by a novel hybrid variational model," *Journal of Visual Communication and Image Representation*, Vol. 22, 2011, pp. 643-652.
14. D. Q. Chen, H. Zhang, and L. Z. Cheng, "A fast fixed point algorithm for total variation deblurring and segmentation," *Journal of Mathematical Imaging and Vision*, Vol. 43, 2012, pp. 167-179.
15. W. Chen, Z.-J. Fu, and C. S. Chen, *Recent Advances in Radial Basis Function Collocation*, Springer, Germany, 2013.
16. Y. Chen, S. Gottlieb, A. Heryudono, and A. Narayan, "A reduced radial basis function method for partial differential equations on irregular domains," *Journal of Scientific Computing*, Vol. 66, 2016, pp. 67-90.

17. A. Chambolle and T. Pock, "A first order primal dual algorithm for convex problems with applications to imaging," *Journal of Mathematical Imaging and Vision*, Vol. 40, 2011, pp. 120-145.
18. M. Dehghan, M. Abbaszadeh, and A. Mohebbi, "A meshless technique based on local radial basis functions collocation method for solving parabolic-parabolic-patlak-keller-segal-chemotaxis model," *Engineering Analysis with Boundary Elements*, Vol. 56, 2015, pp. 129-144.
19. J. M. B. Dias and M. A. T. Figueiredo, "Multiplicative noise removal using variable splitting and constrained optimization," *IEEE Transactions on Image Processing*, Vol. 19, 2010, pp. 1720-1730.
20. F. Dong, H. Zhang, and D. X. Kong, "Nonlocal total variation models for multiplicative noise removal using split bregman iteration," *Mathematical and Computer Modeling*, Vol. 55, 2012, pp. 939-954.
21. T. A. Driscoll and B. Fornberg, "Interpolation in the limit of increasingly at radial basis functions," *Computers and Mathematics with Applications*, Vol. 43, 2002, pp. 413-422.
22. N. Dyn, *Interpolation and Approximation by Radial and Related Function*, Academic Press, Vol. 1, 1989, pp. 211-234.
23. J. Eckstein and D. Bertsekas, "On the Douglas-Rachford splitting method and the proximal point algorithm for maximal monotone operators," *Mathematical Programming*, Vol. 55, 1992, pp. 293-318.
24. E. Esser, X. Zhang, and T. F. Chen, "A general framework for a class of first order primal dual algorithm for convex optimization in imaging sciences," *SIAM Journal on Imaging Sciences*, Vol. 3, 2010, pp. 1015-1046.
25. G. E. Fasshauer, "Solving partial differential equations by collections with radial basis functions," *Proceedings of Chamonix*, 1997, pp. 1-8.
26. A. Golbabai, O. Nikana, and J. R. Tousi, "Note on using radial basis functions method for solving nonlinear integral equations," *Communications in Numerical Analysis*, Vol. 2, 2016, pp. 81-91.
27. E. A. Hale, W. Yin, and Y. Zhang, "Fixed point continuation for l_1 -minimization: Methodology and convergence," *SIAM Journal on Optimization*, Vol. 19, 2008, pp. 1107-1130.
28. L. L. Haung, L. Xiao, and Z. Huiwei, "Multiplicative noise removal via a novel variational model," *EURASIP Journal on Imaging and Video Processing*, Vol. 5, 2010, pp. 987-995.
29. X. Liu and L. Huang, "A new nonlocal total variation regularization algorithm for image denoising," *Mathematics and Computers in Simulation*, Vol. 97, 2014, pp. 224-233.
30. Y. M. Huang, M. K. Ng, and Y. W. Wen, "A new total variation method for multiplicative noise removal," *SIAM Journal on Imaging Sciences*, Vol. 2, 2009, pp. 22-40.
31. S. U. Islam, V. Singh, and S. Rajput, "Estimation of dispersion in an open channel from an elevated source using an upwind local meshless method," *International Journal of Computational Methods*, Vol. 14, 2016.

32. S. U. Islam, B. Sarler, and R. Vertnik, "Local radial basis function collocation method along with explicit time stepping for hyperbolic partial differential equations," *Applied Numerical Mathematics*, Vol. 67, 2013, pp. 136-151.
33. E. J. Kansa, "Multiquadrics – a scattered data approximation scheme with applications to computational fluid dynamics I: Solutions to parabolic, hyperbolic, and elliptic partial differential equations," *Computers and Mathematics with Applications*, Vol. 19, 1990, pp. 147-161.
34. E. J. Kansa, "Multiquadrics – a scattered data approximation scheme with applications to computational fluid dynamics II: Surface approximations and partial derivative estimates," *Computers and Mathematics with Applications*, Vol. 19, 1990, pp. 127-145.
35. E. J. Kansa, *Motivation for Using Radial Basis Functions to Solve PDEs*, Lawrence Livermore National Library, USA, 1999.
36. M. A. Khan, W. Chen, and A. Ullah, and Z. Fu, "A mesh-free algorithm for ROF model," *EURASIP Journal on Advances in Signal Processing*, Vol. 2017, 2017, pp. 1-16.
37. E. Larsson and B. Fornberg, "A numerical study of some radial basis function based solution methods for elliptic PDEs," *Computers and Mathematics with Applications*, Vol. 46, 2003, pp. 891-902.
38. E. Larsson and B. Fornberg, "On the efficiency and exponential convergence of multiquadric collocation method compared with finite element method," *Engineering Analysis with Boundary Elements*, Vol. 27, 2003, pp. 251-257.
39. J. Li and Y. C. Hon, "Domain decomposition for radial basis meshless methods," *IEEE Transactions on Communications*, Vol. 31, 1983, pp. 388-397.
40. K. Liu, "Radial basis functions: Biomedical applications and parallelization," *Theses and Dissertations*, University of Wisconsin-Milwaukee, 2016.
41. W. R. Madych and S. A. Nelson, "Multivariate interpolation: a variational theory," *Mathematics of Computation*, Vol. 54, 1990, pp. 211-230.
42. A. Marquina, S. Osher, "Explicit algorithms for a new time dependent model based on level set motion for nonlinear deblurring and noise removal," *SIAM Journal on Scientific Computing*, Vol. 22, 2000, pp. 387-405.
43. C. A. Micchelli, "Interpolation of scattered data: Distance matrices and conditionally positive definite functions," *Constructive Approximation*, Vol. 2, 1986, pp. 11-22.
44. G. Narkiss and M. Zibulevsky, "Sequential subspace optimization method for large scale unconstrained problem," *Cite Seer*, 2005.
45. M. K. Ng, L. O. Qi, Y. F. Yang, and Y. M. Huang, "On semi-smooth Newton's methods for total variation minimization," *Journal of Mathematical Imaging Vision*, Vol. 27, 2007, pp. 265-276.
46. T. Pock and A. Chambolle, "Diagonal preconditioning for the first order primal dual algorithms in convex optimization," in *Proceedings of International Conference on Computer Vision*, 2011, pp. 762-769.
47. L. I. Rudin, S. Osher, and E. Fatemi, "Nonlinear total variation based noise removal algorithms," *Physica D: Nonlinear Phenomena*, Vol. 60, 1992, pp. 259-268.
48. L. I. Rudin, P. L. Lions, and S. Osher, "Multiplicative denoising and deblurring: theory and algorithms," *Geometric Level Set Methods in Imaging Vision and Graphics*, Vol. 3, 2003, pp. 103-119.

49. L. I. Rudin and S. Osher, "Total variation based image restoration with free local constraints," *IEEE Transactions on Image Processing*, Vol. 1, 1994, pp. 31-35.
50. L. I. Rudin, P. L. Lions, and S. Osher, "Multiplicative denoising and deblurring: theory and algorithms," *Geometric Level Set Methods in Imaging, Vision, and Graphics*, Springer, Berlin, 2003, pp. 103-120.
51. S. A. Sarra, "Multiquadric radial basis function approximation methods for the numerical solution of partial differential equations," *Artical*, Marshall University and Edward J. Kansa, University of California, 2009.
52. S. A. Sarra, "Digital total variation filtering as postprocessing for Chebyshev pseudospectral methods for conservation laws," *Numerical Algorithms*, Vol. 41, 2005, pp. 17-33.
53. S. A. Sarra, "Digital total variation filtering as postprocessing for radial basis function approximation methods," *Computers and Mathematics with Applications*, Vol. 52, 2006, pp. 1119-11130.
54. R. Schaback, "A practical guide to radial basis functions," *Artical*, Springer, 2007.
55. M. G. Shama, T. Z. Huang, J. Liu, and S. Wang, "A convex total variation generalization regularized model for multiplicative noise and blur removal," *Applied Mathematics and Computation*, Vol. 276, 2016, pp. 109-121.
56. C. Sheng, Y. Xin, Y. Liping, and S. Kun, "Total variation-based speckle reduction using multi-grid algorithm for ultrasound Images," *Image Analysis and Processing*, 2005, pp. 245-252.
57. B. Shi, L. Haung, and Z. F. Pang, "Fast algorithm for multiplicative noise removal," *Journal of Visual Communication and Image Representation*, Vol. 23, 2012, pp. 126-133.
58. J. Shi and S. Osher, "A nonlinear inverse scale space method for a convex multiplicative noise model," *SIAM Journal on Imaging Sciences*, Vol. 1, 2008, pp. 294-321.
59. G. Steidl and T. Teuber, "Removing multiplicative noise by Douglas-Rachford splitting methods," *Journal of Mathematical Imaging and Vision*, Vol. 36, 2010, pp. 168-184.
60. J. Sun, Q. Zhang, F. Wang, and X. Zhao, "On the generalization of digital total variation filter," *Image and Signal Processing*, Vol. 3, 2008, pp. 384-388.
61. D. Tian, Y. Du, and D. Chen, "An adaptive fractional-order variation method for multiplicative noise removal," *Journal of Information Science and Engineering*, Vol. 32, 2016, pp. 747-762.
62. A. Ullah, W. Chen, and M. A. Khan, "A new variational approach for restoring images with multiplicative noise," *Computers and Mathematics with Applications*, Vol. 71, 2016, pp. 2034-2050.
63. X. Wang, Y. Bi, X. Feng, and L. Huo, "Multiplicative noise removal using primal-dual and reweighted alternating minimization," *SpringerPlus*, Vol. 5, 2016, p. 5:277.
64. G. B. Wright, "Radial basis function interpolation: numerical and analytical developments," Ph.D. Thesis, Department of Applied Mathematics, University of Colorado, 2008.
65. S. Wright, M. Zhu, and T. Chen, "Duality based algorithms for total variation regularized image restoration," *Computational Optimization and Applications*, Vol. 47, 2010, pp. 377-400.

66. S. Wright, R. Nowak, and M. Figueiredo, "Sparse reconstruction by separable approximation," *IEEE Transactions on Signal Processing*, Vol. 57, 2009, pp. 2479-2493.
67. H. Woo and S. Yun, "Proximal linearized alternating direction method for multiplicative denoising," *SIAM Journal on Scientific Computing*, Vol. 35, 2013, pp. 336-358.
68. H. Xie, L. E. Pierce, and F. T. Ulaby, "SAR speckle reduction using wavelet denoising and Markova random field modeling," *IEEE Transactions on Geoscience and Remote Sensing*, Vol. 40, 2002, pp. 2196-2212.
69. M. Zerroukat, H. Power, and C. S. Chen, "A numerical method for heat transfer problem using collocation and radial basis functions," *International Journal for Numerical Methods in Engineering*, Vol. 42, 1998, pp. 1263-1278.
70. Q. Zhang, J. Sun, and G. Xu, "Noise removal based on the variation of digitized energy," *GMP, Advances in Geometric Modeling and Processing*, Vol. 4975, 2008, pp. 290-303.
71. M. Zhou and T. Chen, "An efficient primal dual hybrid gradient algorithm for total variation image restoration," Technical Report No. 03-34, UCLA, 2008, pp. 8-34.



Mushtaq Ahmad Khan is currently doing Ph.D. from School of Engineering Mechanics and Materials, Hohai University, Nanjing, China. His research interest includes image restoration and radial basis function approximation.



Wen Chen has done his Ph.D. in Fluid Transmission and Control, Department of Mechanical Engineering, Shanghai Jiao Tong University 1997. Currently, he is a Professor in the School of Engineering Mechanics and Materials, Hohai University, Nanjing, China. His current research consists of the two major directions: (1) Scientific Computing and Computational Mechanics, involving radial basis function methods, differential quadrature method, inverse elastodynamic and heat conduction problems, nonlinear dynamics; (2) Mechanics and physics of soft matter (*e.g.*, polymers, colloids, emulsions, foams, living organisms, rock layers, sediments, plastics, glass, rubber, oil, soil, DNA) and their mathematical modeling, involving modeling of medical ultrasonic imaging, fractional and fractal calculus, mesoscopic physics, Levy statistics and fractional Brownian motion, anomalous diffusions (frequency-dependent dissipation and damping).



Zhuojia Fu received his Ph.D. degree in Engineering Mechanics from Hohai University, China, in 2013. He is now a Professor in the College of Mechanics and Materials at Hohai University, China. His current research interests include semi-analytical and numerical methods in computational mechanics, numerical modeling of wave propagation and structural vibration, engineering inverse analysis.



Asmat Ullah has done his Ph.D. from School of Engineering Mechanics and Materials, Hohai University, Nanjing, China in 2017. He is now the Subject Specialist in Mathematics at E and S Education Department KPK, Peshawar, Pakistan. His research interest includes image restoration and fractional order derivatives.